

## Supplementary Tables and Figures

### Designing a chemical inhibitor for the AAA protein spastin using silent mutations

Tommaso Cupido<sup>1</sup>, Rudolf Pisa<sup>1,2</sup>, Megan E. Kelley<sup>1</sup>, and Tarun M. Kapoor<sup>1\*</sup>

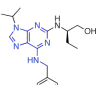
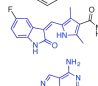
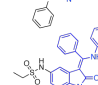
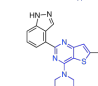
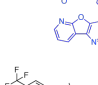
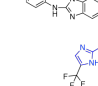
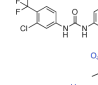
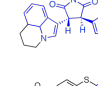
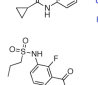
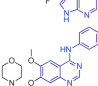
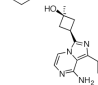
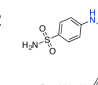
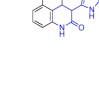


<sup>1</sup>The Rockefeller University, Laboratory of Chemistry and Cell Biology, The Rockefeller University, New York, New York, 10065, USA. <sup>2</sup>Tri-Institutional PhD program in Chemical Biology, The Rockefeller University, New York, New York, 10065, USA.

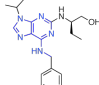
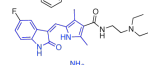
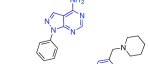
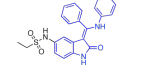
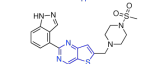
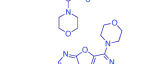
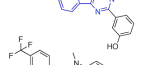
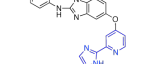
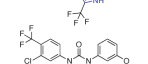
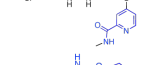
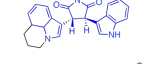
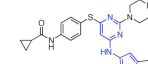
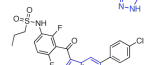
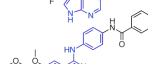
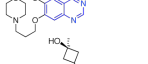
\*e-mail: kapoor@rockefeller.edu

#### Table of Contents

Supplementary Table 1	_____ pg	2
Supplementary Table 2	_____ pg	4
Supplementary Table 3	_____ pg	5
Supplementary Table 4	_____ pg	6
Supplementary Figure 1	_____ pg	7
Supplementary Figure 2	_____ pg	9
Supplementary Figure 3	_____ pg	11
Supplementary Figure 4	_____ pg	12
Supplementary Figure 5	_____ pg	14

**Supplementary Table 1. Compounds tested against AAA proteins (supporting data for Fig. 2c).** Each compounds' chemical structure, name, IUPAC chemical identifier, kinase-bound PDB code, vendor, and purity information are shown. PDB structures were used to analyze potential hydrogen bonds between protein kinases and compounds' core heterocycle (highlighted in blue).

	structure	name	International Chemical Identifier	PDB	Vendor (catalog number)	Purity (HPLC)
22		Seliciclib	BTIHMVBBUGXLCJ-OAHLLOKOSA-N	2A4L	LC Laboratories (R-1234)	>95%
23		Sunitinib	WINHZLLDWRZWRT-ATVHPVEESA-N	3G0E	LC Laboratories (S8877)	>95%
24		PP3	KKDPIZPUTYIBFX-UHFFFAOYSA-N	4GKH	Tocris (2794)	>95%
25		Hesperadin	GLDSKRNGVYJAB-DQSJHHFOSA-N	2BFX	Selleck (S1529)	>95%
26		Pictilisib	LHNIIDJUOCFXAP-UHFFFAOYSA-N	2WXP	LC Laboratories (G-9252)	>95%
27		PI-103	TUVCWJQQGGETHL-UHFFFAOYSA-N	4L23	LC Laboratories (P-9099)	>95%
28		CHIR265	YABJJWZLRMPFSI-UHFFFAOYSA-N	5CT7	Selleck (S2161)	>95%
29		Sorafenib	MLDQJTXFUGDVEQ-UHFFFAOYSA-N	1UWH	Selleck (S7397)	>95%
30		Tivantinib	UCEQXRCJXIVODC-PMACEKPBSA-N	3RHK	Selleck (S2753)	>95%
31		Tozasertib	GCIKSSRWFVXBI-UHFFFAOYSA-N	4AF3	LC Laboratories (T-2304)	>95%
32		Vemurafenib	GPXBXXGIAQBQNI-UHFFFAOYSA-N	4RZV	ChemScene (CS-0216)	>95%
33		ZM-447439	OGNYUTNQZVRGMN-UHFFFAOYSA-N	2VRX	Tocris (2458)	>95%
34		Linsitinib	PKCDDUHJAFVJJB-UHFFFAOYSA-N	N.A.	Selleck (S1091)	>95%
compound 2		JNJ-7706621	KDKUVYLMPIJGKA-UHFFFAOYSA-N	5USY	ApexBio (A4115)	>95%
35		Dovitinib	KCOYQXZDIIGCY-ZZEZOPTASA-N	5A46	Selleck (S1018)	>95%

	structure	name	International Chemical Identifier	PDB	Vendor (catalog number)	Purity (HLPC)
22		Seliciclib	BT1HMVBBUGXLCJ-OAHLLOKOSA-N	2A4L	LC Laboratories (R-1234)	>95%
23		Sunitinib	WINHZLLDWRZWRT-ATVHPVEESA-N	3G0E	LC Laboratories (S8877)	>95%
24		PP3	KKDPIZPUTYIBFX-UHFFFAOYSA-N	4GKH	Tocris (2794)	>95%
25		Hesperadin	GLDSKRNQVWYJAB-DQSJHHFOSA-N	2BFX	Selleck (S1529)	>95%
26		Pictilisib	LHNIIDJUCFXAP-UHFFFAOYSA-N	2WXP	LC Laboratories (G-9252)	>95%
27		PI-103	TUVVQJQQGETHL-UHFFFAOYSA-N	4L23	LC Laboratories (P-9099)	>95%
28		CHIR265	YABJWZLRMPFSI-UHFFFAOYSA-N	5CT7	Selleck (S2161)	>95%
29		Sorafenib	MLDQJTXFUGDVEO-UHFFFAOYSA-N	1UWH	Selleck (S7397)	>95%
30		Tivantinib	UCEQXRCJXIVODC-PMACEKPBSA-N	3RHK	Selleck (S2753)	>95%
31		Tozasertib	GCIKSSRWRFVXBI-UHFFFAOYSA-N	4AF3	LC Laboratories (T-2304)	>95%
32		Vemurafenib	GPXBXXGIAQBQNI-UHFFFAOYSA-N	4RZV	ChemScene (CS-0216)	>95%
33		ZM-447439	OGNYUTNQZVRGMN-UHFFFAOYSA-N	2VRX	Tocris (2458)	>95%
34		Linsitinib	PKCDDUJAFVJJB-UHFFFAOYSA-N	N.A.	Selleck (S1091)	>95%
compound 2		JNJ-7706621	KDKUVVYLMPIJGKA-UHFFFAOYSA-N	5USY	ApexBio (A4115)	>95%
35		Dovitinib	KCOYQXZDFIIGCY-ZZEZOPTASA-N	5A46	Selleck (S1018)	>95%

**Supplementary Table 2. Structure-activity relationship analysis of compound 1 derivatives (supporting data for Fig. 2).** Six compound 1 analogs were generated using readily available commercial building blocks. Core structures and corresponding variable groups ( $R_n$ ) of the synthesized compounds are shown. Compounds were tested against Dm-spastin ( $n=2$ ) and average percent ATPase activity values, normalized to the DMSO control, were used to score compound-mediated inhibition (see legend in Supplementary Table 2).

Core structure		$R_1$	$R_2$	entry	[compound] = 10 $\mu$ M
				8	-
				9	+
				10	++
				11	-
				12	-
				13	+

Legend	
Dm-spastin ATPase activity % of control	score
< 21	++
21-70	+
71-100	-

**Supplementary Table 3. Amino acids found at the P-loop variability hot-spot position in human AAA proteins (supporting data for Fig. 4).** Sequence for AAA proteins were obtained as follows: in Uniprot.org, a search was performed using “ipr003959”, “ipr003593”, and “human” keywords. The P-loop variability hot-spot residue was identified using the uniprot nucleotide binding function as the fifth residue (n) of the GPxGnGKx consensus sequence (x = variable residue).

N	GENE NAME	AA	N	GENE NAME	AA	N	GENE NAME	AA
1	AFG32=	Thr	31	LONM=	Val	61	PSMC1=	Thr
2	ATAD1=	Cys	32	LONP1 =	Val	62	PSMC3=	Thr
3	ATAD2=	Thr	33	MCM2 =	Thr	63	PSMC4=	Cys
4	ATAD5=	Thr	34	MCM3 =	Val	64	PSMC5=	Thr
5	ATD2B=	Thr	35	MCM4 =	Thr	65	PSMC8=	Thr
6	ATD3A=	Thr	36	MCM5 =	Thr	66	RFC1 =	Thr
7	ATD3B=	Thr	37	MCM5 =	Thr	67	RFC2 =	Thr
8	ATD3C=	Thr	38	MCM6 =	Thr	68	RFC3 =	Ala
9	BCS1L=	Cys	39	MCM7 =	Val	69	RFC4 =	Thr
10	CDC6 =	Thr	40	MCM8 =	Leu	70	RUVBL1 =	Thr
11	CLPB=	Ile	41	MCM9 =	Thr	71	RUVBL2=	Thr
12	CLPX =	Ser	42	MDN1 (D1) =	Cys	72	SMBP=	Thr
13	CTHF18 =	Leu	43	MDN1 (D2) =	Thr	73	SPASL (D1)=	Val
14	DYNC1H1 (D1) =	Thr	44	MDN1 (D3) =	Val	74	SPASL (D2)=	Cys
15	DYNC1H1 (D2) =	Ser	45	MDN1 (D4) =	Cys	75	SPAT5 (D1)=	Cys
16	DYNC1H1 (D3) =	Ser	46	MDN1 (D5) =	Val	76	SPAT5 (D2)=	Thr
17	DYNC1H1 (D4) =	Ala	47	MDN1 (D6) =	Val	77	SPG7=	Cys
18	DYNC2H1 (D1) =	Thr	48	NSF (D1) =	Cys	78	<b>SPASTIN =</b>	<b>Asn</b>
19	DYNC2H1 (D2) =	Ala	49	NSF (D2) =	Ser	79	TERA (VCP) (D1) =	Thr
20	DYNC2H1 (D3) =	Cys	50	NVL (D1) =	Cys	80	TERA (VCP) (D2) =	Cys
21	DYNC2H1 (D4) =	Val	51	NVL (D2) =	Cys	81	TOR1B =	Thr
22	FIGL1=	Thr	52	ORC1 =	Thr	82	TOR2A =	Thr
23	FIGL2=	Thr	53	ORC4=	Ser	83	TOR4A =	Val
24	FIGN=	Thr	54	ORC5 =	Ser	84	VPS4 =	Thr
25	IQCA1=	Val	55	PCH2 =	Thr	85	VPS4A=	Thr
26	HELZ2 (D1)=	Thr	56	PEX1 (D1)=	Thr	86	VPS4B =	Thr
27	HELZ2 (D2)=	Thr	57	PEX1 (D2) =	Ser	87	VWA8 (D1) =	Cys
28	KATL1=	Thr	58	PEX6 (D1)=	Thr	88	VWA8 (D2) =	Val
29	KATL2=	Thr	59	PEX6 (D2)=	Cys	89	WRNIP1 =	Cys
30	KATNA1=	Thr	60	PMSC2=	Thr	90	YME1-like1 =	Thr

### Supplementary Table 4. Activity of compound 6 and compound 7 against kinases.

Heat-map for the inhibition of 64 human kinases by compounds 6 and 7 (2  $\mu$ M). Heat map was constructed from average percent kinase activity inhibition values in the presence of the compound (n = 2) normalized to DMSO control (see legend). To assess kinase activity we used the commercial Z'-LYTE platform (Thermofisher). ATP concentration in the kinase reactions was 1 mM, matching that used in all ATPase assays with Hs-spastin constructs.

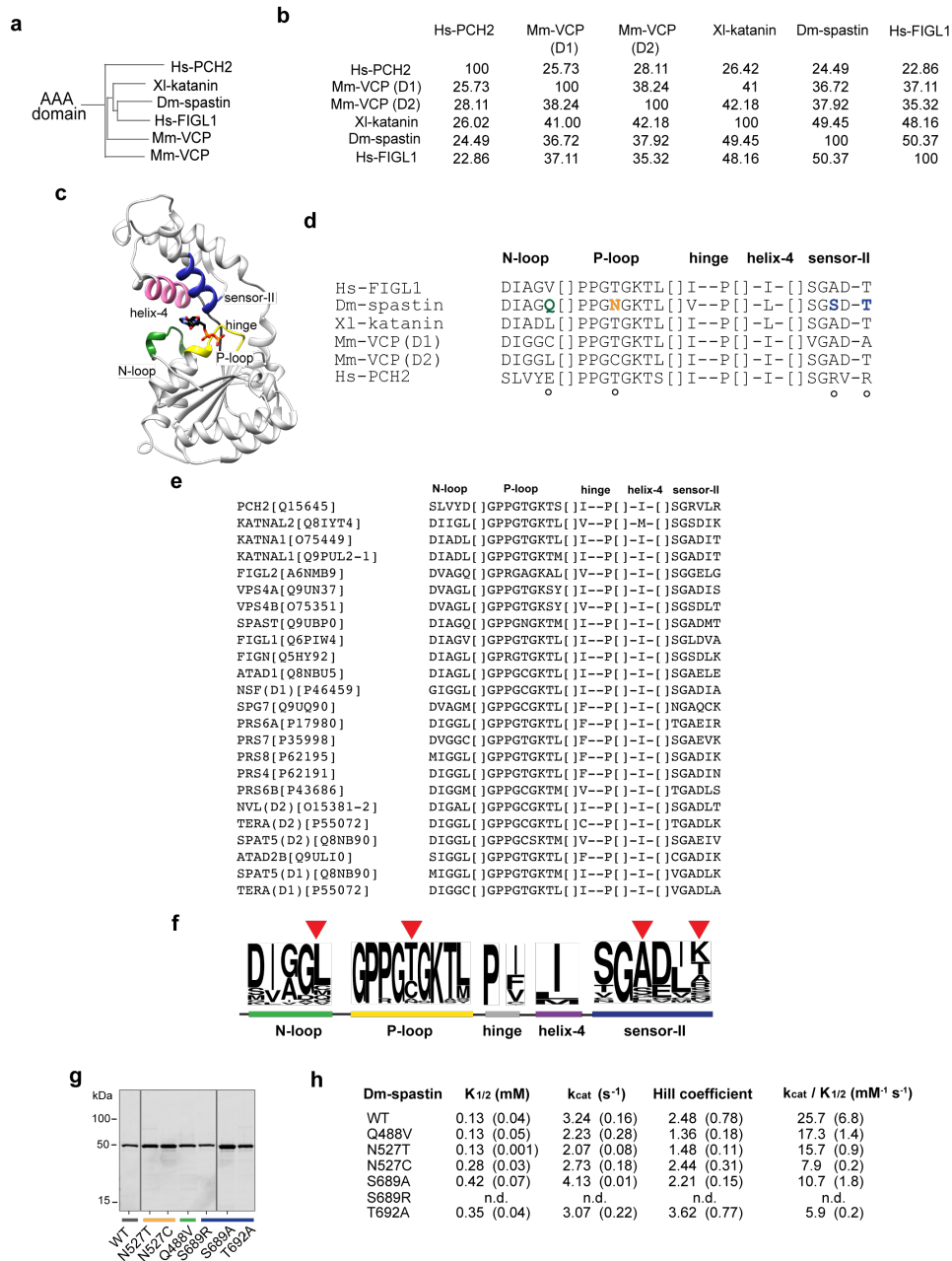
ATP conc	Kinase	comp. 6	comp. 7
$\mu$ M			
1 1000	ABL1	9	1
2 1000	AKT1 (PKB alpha)	6	2
3 1000	ALK	11	4
4 1000	AURKA (Aurora A)	-5	1
5 1000	AURKB (Aurora B)	0	6
6 1000	AURKC (Aurora C)	-	2
7 1000	BTK	10	-3
8 1000	CAMK2A (CaMKII alpha)	-2	6
9 1000	CDK2/cyclin A	1	3
10 1000	CDK5/p25	1	1
11 1000	CHEK1 (CHK1)	8	1
12 1000	CHEK2 (CHK2)	40	1
13 1000	CSF1R (FMS)	20	19
14 1000	CSNK1A1 (CK1 alpha 1)	-3	3
15 1000	CSNK1G2 (CK1 gamma 2)	1	-2
16 1000	CSNK2A2 (CK2 alpha 2)	-1	1
17 1000	DYRK1A	4	1
18 1000	EGFR (ErbB1)	4	0
19 1000	EPHA2	1	0
20 1000	FER	8	5
21 1000	FGFR1	17	16
22 1000	FLT3	70	44
23 1000	FLT4 (VEGFR3)	-2	-1
24 1000	FRAP1 (mTOR)	-3	2
25 1000	GSK3A (GSK3 alpha)	8	0
26 1000	GSK3B (GSK3 beta)	23	9
27 1000	IKBKE (IKK epsilon)	1	-1
28 1000	INSR	5	9
29 1000	IRAK4	10	10
30 1000	JAK1	8	3
31 1000	JAK2	6	-2
32 1000	KDR (VEGFR2)	8	1
33 1000	LCK	15	2
34 1000	LYN A	14	7
35 1000	MAP3K9 (MLK1)	67	8
36 1000	MAP4K4 (HGK)	23	7
37 1000	MAPK1 (ERK2)	-3	11
38 1000	MAPK14 (p38 alpha) Direct	-4	8
39 1000	MAPKAPK2	2	3
40 1000	MARK1 (MARK)	6	6
41 1000	MET (cMet)	13	4
42 1000	MINK1	2	5
43 1000	MST4	-21	-14
44 1000	MYLK2 (skMLCK)	2	3
45 1000	NEK2	15	10
46 1000	NTRK1 (TRKA)	72	65
47 1000	PAK4	13	5
48 1000	PDK1 Direct	14	1
49 1000	PIM2	8	3
50 1000	PRKACA (PKA)	5	6
51 1000	PRKCA (PKC alpha)	9	10
52 1000	PRKCA (PKC Beta I)	20	2
53 1000	PRKCD (PKC delta)	-1	8
54 1000	PRKD2 (PKD2)	8	4
55 1000	ROCK1	4	1
56 1000	RPS6KA1 (RSK1)	31	16
57 1000	RPS6KA2 (RSK3)	59	16
58 1000	RPS6KB1 (p70S6K)	10	2
59 1000	SGK (SGK1)	12	0
60 1000	SRC	28	6
61 1000	STK3 (MST2)	-3	3
62 1000	TAOK2 (TAO1)	31	11
63 1000	TBK1	2	1
64 1000	TEK (Tie2)	12	1
65 1000	TYK2	9	2

[compound] = 2  $\mu$ M

< 30%  
 30 to 50%  
 > 50%

% Inhibition of control activity

## Supplementary Figure 1

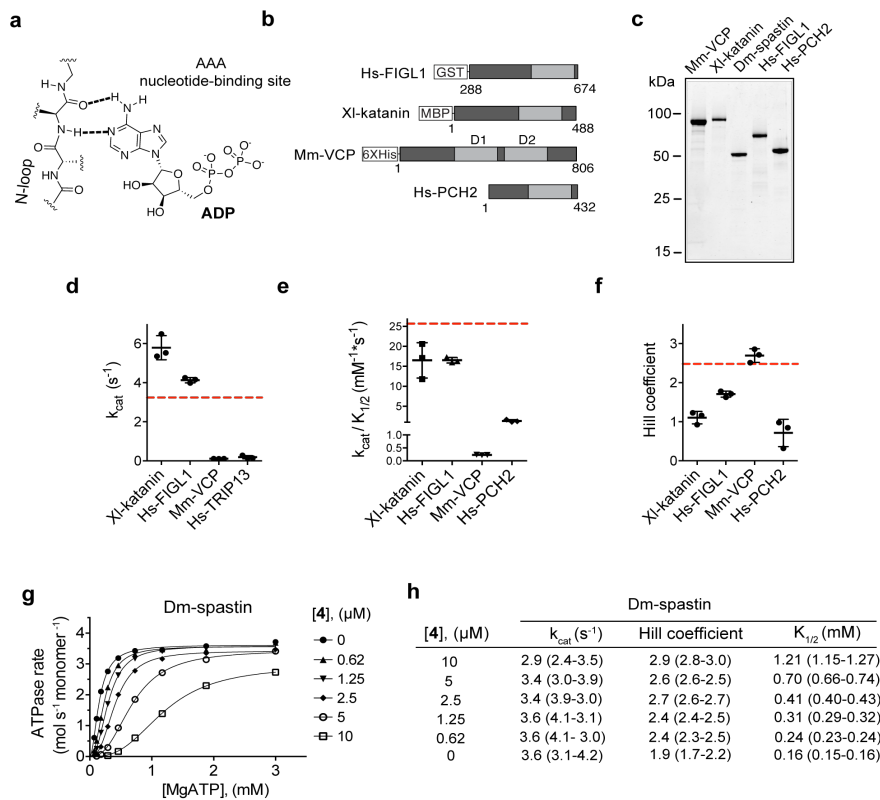


**Supplementary Figure 1: Analysis of primary sequence similarity in AAA proteins and characterization of Dm-spastin variability hot-spot mutants (supporting data for Fig. 1).** (a) A sequence similarity tree diagram of the AAA domains of PCH2 (*Homo sapiens*, Hs, Uniprot:Q15645, aa 131-422), katanin (*Xenopus laevis*, Xl, Uniprot:Q9PUL2, aa 199-481), spastin (*Drosophila melanogaster*, Dm, Uniprot:Q810P1,

aa 477-749), FIGL1 (Hs, Uniprot:Q6PIW4, aa 395-666), , and VCP (*Mus musculus*, Mm, Uniprot:Q01853, N-terminal [D1, aa 198-470] and C-terminal [D2, aa 471-758] domains). (b) Pairwise sequence identity matrix, generated using multiple sequence alignment in Clustal  $\Omega$ , for the AAA domains in five AAA proteins. (c) Structural model (ribbon diagram) of a AAA domain (human FIGL1, PDB:3D8B). The structural motifs of the nucleotide-binding site are highlighted (N-loop: green, P-loop: yellow, helix-4: magenta, sensor-II: blue, hinge: dark gray). ADP is also shown (stick representation). (d) Within these five structural motifs of Hs-FIGL1, the residues that are  $< 6 \text{ \AA}$  from the adenine were selected and aligned with residues at equivalent positions in the other four AAA proteins (VCP contains two AAA domains). The alignment shown in d was used to construct the sequence logo diagram in Fig. 1b. Dashes indicate residues that are not shown as they are  $> 6 \text{ \AA}$  from the adenine, and closed square brackets indicate sequence gaps of variable length. Selected non-conserved amino acid positions are highlighted (variability hot-spots, colored as in Fig. 1). (e) Sequence alignment of the residues in the N-loop, P-loop, hinge, helix-4 and sensor-II motifs of 24 AAA domains from human AAA proteins (Uniprot sequence identifiers are indicated in square brackets). (f) Sequence logo diagram for the 24 AAA domains in e, showing the relative frequency of amino acids at each position. Arrows indicate variability hot-spot amino acid positions. (g) SDS-PAGE analysis of purified wildtype (WT) and mutant Dm-spastin constructs (Coomassie blue, gels for purified proteins were run at least twice). (h) Analysis of the steady-state ATPase activity of Dm-spastin wildtype (WT) and mutant constructs (supporting data for Fig. 1d-1g). Values for enzyme activity parameters are provided (average,  $n = 3$ , s.d. in parentheses). Rates were plotted against MgATP concentration and data were fit to the Michaelis-Menten equation for cooperative enzymes (see Online Methods). The data from each experiment were fit separately and the values, as determined by the fitting, were averaged.



## Supplementary Figure 2

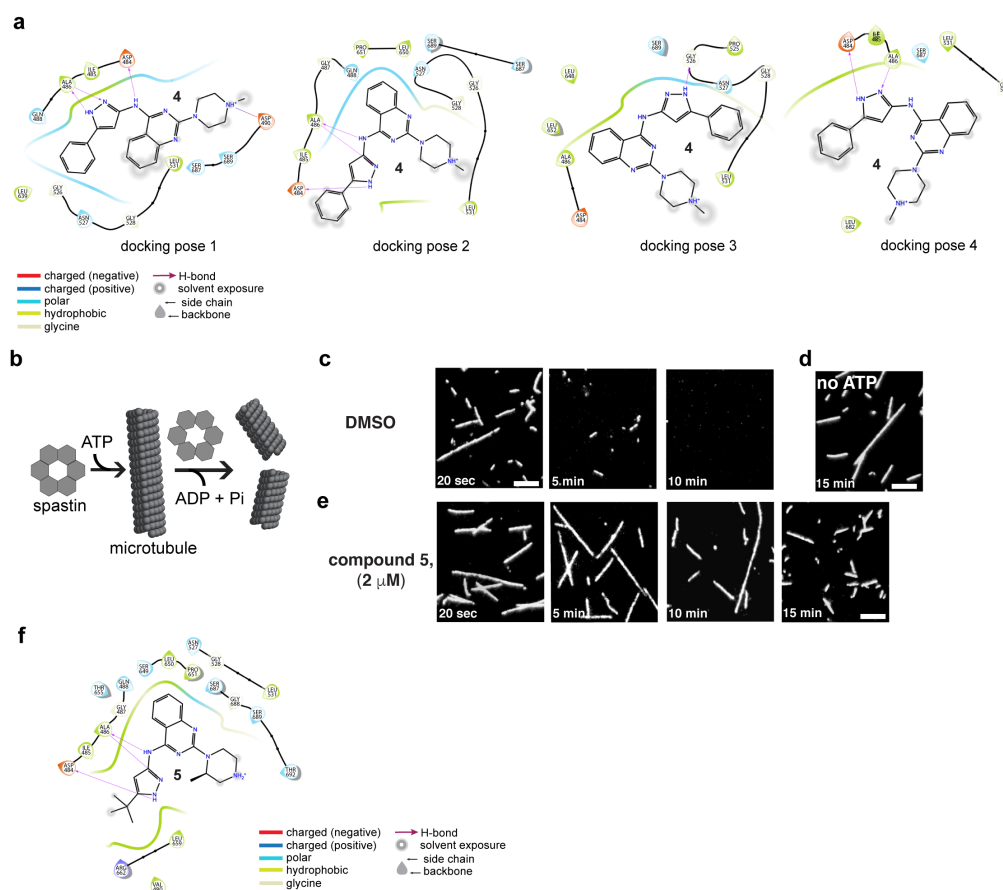


### Supplementary Figure 2: Characterization of four AAA proteins (supporting data for Fig. 2).

(a) Schematic for the predicted hydrogen-bonding interactions (dashed lines) between adenine and the N-loop in AAA proteins. (b) Schematic shows the AAA domain (light gray boxes), tags for affinity purification, and the first and last residues of four AAA protein constructs (not to scale). (c) SDS-PAGE analysis of purified recombinant AAA proteins, including Dm-spastin, Mm-VCP/p97, XI-katanin, Hs-FIGL1, Hs-PCH2 (Coomassie blue, gels for purified proteins were run at least twice). (d-f) Graphs show values for the catalytic turnover ( $k_{cat}$ ; d), catalytic efficiency ( $k_{cat}/K_{1/2}$ ; e), and Hill coefficients (f). Lines represent average  $\pm$  s.d. ( $n=3$ ). The corresponding values for the Dm-spastin construct are also indicated (red dashed line, data from Fig. 1d, 1f and 1g). (g) ATP concentration-dependence of the steady-state ATPase activity of Dm-spastin at different concentrations of compound (average,  $n = 2$ ) (h) Values for Dm-spastin enzyme

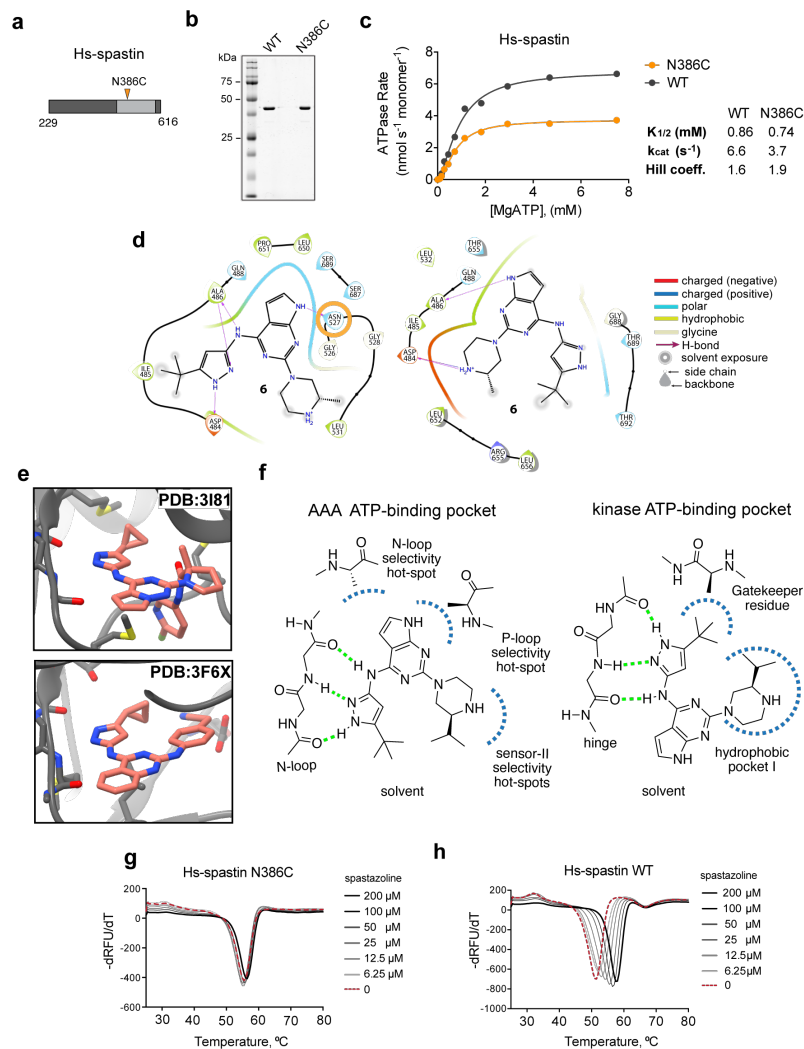
activity parameters in the presence of compound **4** at the indicated concentrations are provided (average, n = 2, range in parentheses). Range of MgATP concentrations tested was 0.027 to 3 mM. Steady-state ATPase activity was analyzed using an NADH-coupled assay. To calculate enzyme parameters, rates were plotted against MgATP concentration and data were fit to the Michaelis-Menten equation for cooperative enzymes. The data from each experiment were fit separately and the values, as determined by the fitting, were averaged.

### Supplementary Figure 3



**Supplementary Figure 3: Analyses of compound binding and inhibition of Dm-spastin (supporting data for Fig. 3).** (a) Four computational docking models for compound **4** bound to the spastin nucleotide-binding site. Diagrams show the inhibitor surrounded by protein residues found within 3.0 Å of the inhibitor. Relevant inhibitor-spastin interactions are indicated (see legend in the figure). Models were generated from the atom coordinates of the inhibitor-spastin computational docking complexes, using the Ligand Interaction function in Schrodinger Maestro. (b) Schematic for a microtubule-severing reaction. (c-e) An assay was used to test inhibition of Dm-spastin microtubule-severing activity by compound **5**. Representative fluorescence microscopy images (n=2) of rhodamine-labeled taxol-stabilized microtubules incubated with Dm-spastin (15 nM) and DMSO (1%, c and d) or compound **5** (e) for the indicated times, in the presence (c and e) or absence (d) of MgATP (0.5 mM). Scale bar = 2  $\mu$ m. (f) Model for compound **5** bound to the Dm-spastin nucleotide-binding site. Diagram was generated as described in a.

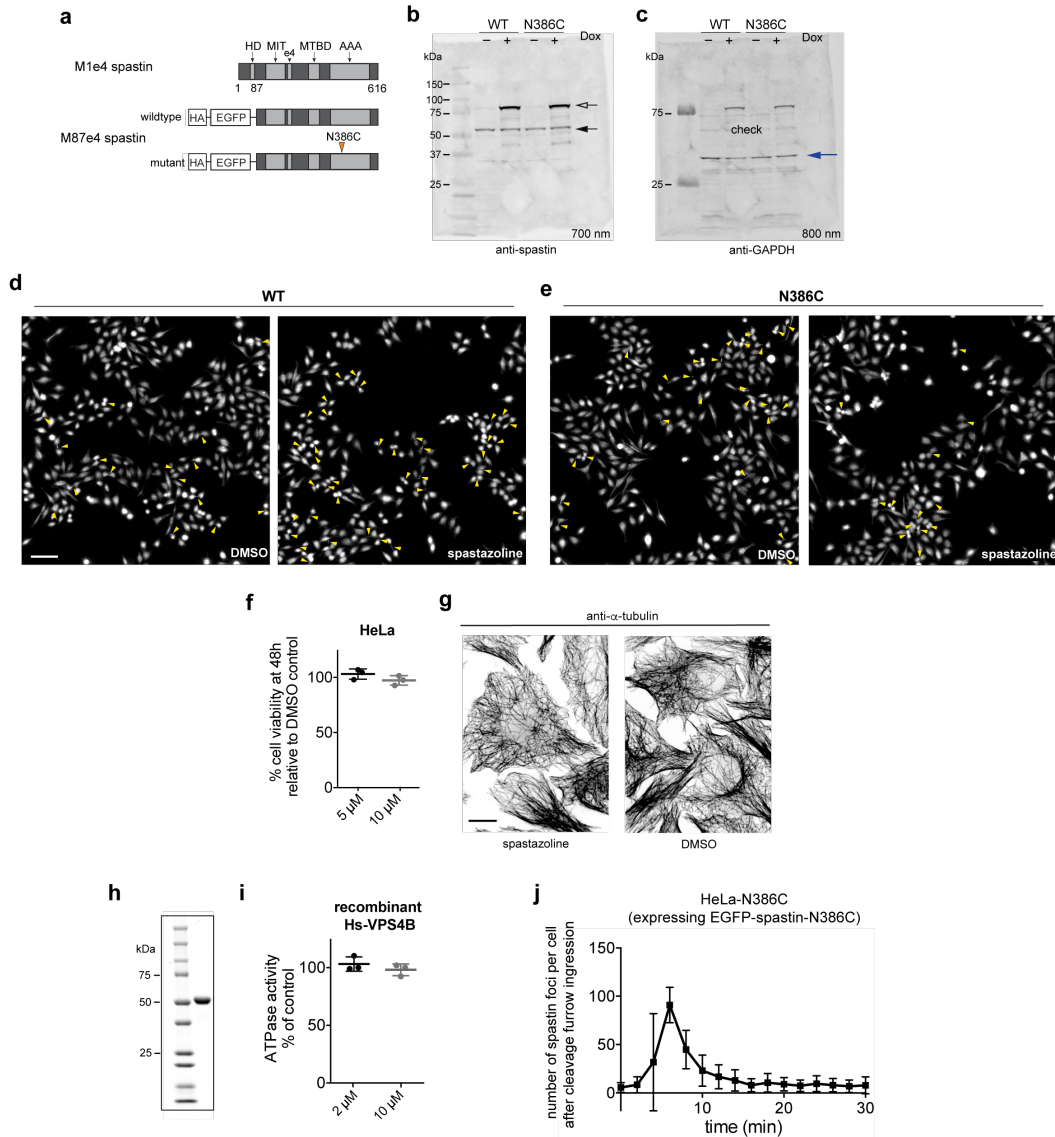
## Supplementary Figure 4



**Supplementary Figure 4: Design of a potent Hs-spastin inhibitor and its cognate resistance-conferring mutation (supporting data for Fig. 4).** (a) Schematic shows AAA domain (light gray box, not to scale) and the first and last residues of the recombinant Hs-spastin wild-type of N386C mutant constructs. The position of the N386C mutation is indicated with an orange arrow. (b) SDS-PAGE analysis of purified recombinant wild-type (WT) and mutant (N386C) Hs-spastin (Coomassie blue, gels for purified proteins were run at least twice). (c) ATP concentration-dependence of the steady-state activity of the Hs-spastin wild-type (WT) and mutant (N386C) constructs, analyzed using an NADH-coupled assay. Averages ( $n = 2$ ) were fit to the Michaelis-Menten equation for cooperative enzymes. Measured values for enzyme activity

parameters are provided. To calculate enzyme activity parameters data from each experiment were fit separately and the values, as determined by the fitting, were averaged. **(d)** Diagrams show two computational docking models for compound **6** bound to the Dm-spastin nucleotide-binding site. The protein residues within 3.0 Å of compound **6** and relevant compound-protein interactions are indicated (see legend in the figure). The position of the P-loop variability hot-spot residue is also shown (orange circle). **(e)** X-ray structural models for a 4-pyrazolyl, 2-substituted-triazine-based compound (top panel), and a 4-pyrazolyl, 2-substituted-quinazoline-based compound (bottom panel) bound to protein kinases (compounds: stick representations, carbon atoms in orange; kinase: ribbon and stick representations; PDB codes are indicated). **(f)** Schematics show likely orientations of spastazoline bound to AAA proteins (left) or kinases (right). Selected protein structural motifs that interact with the inhibitor are indicated. **(g-h)** Differential scanning fluorimetry analysis of spastazoline-dependent changes in the melting temperature of Hs-spastin N386C mutant (N386C, **g**) or wildtype (WT, **h**) in 2% DMSO alone (red dashed lines) or with spastazoline (grayscale lines). Representative experiments are shown (n=3). Average melting temperature with DMSO control for N386C: 54.5 °C, range 54.0-54.5 °C, for WT: 51.5 °C, range 51.5-51.5 °C. Average shift in melting temperature in the presence of spastazoline (200 µM) for N386C: 1.5 °C, range 1.0-1.5 °C; for WT: 6 °C, range 6.0-6.5 °C, n = 3).

## Supplementary Figure 5



**Supplementary Figure 5: Analysis of spastin-dependent phenotypes in HeLa cells treated with spastazoline (supporting data for Fig. 5).** (a) Schematics for the spastin M1e4 and M87e4 isoforms. Structural domains, along with the mutation (orange arrow) and tags for the M87e4 isoform expressed in HeLa cells are indicated (not to scale). (b-c) Immunoblot analysis of HeLa cells expressing wildtype (WT) or N386C mutant (N386C) spastin M87e4 constructs. Doxycycline (1  $\mu\text{g}/\text{mL}$ , 24 hours) was used to induce expression and blots were stained for spastin (b) and GAPDH (c) as a loading control. The positions of the bands expected for the GFP-spastin constructs and the endogenous

spastin (outlined and black arrows, respectively), or for GAPDH (blue arrow) are indicated. These experiments were repeated twice. **(d-e)** Representative images of fixed, doxycycline-induced WT and N386C cells treated with DMSO (0.1%) or spastazoline (10  $\mu$ M) for 4.5 hours, and stained for acetylated tubulin. Yellow arrows indicate intercellular bridges. Scale bar = 100  $\mu$ m **(f)** Analysis of cell viability in HeLa-WT cells treated with spastazoline for 48 h at the indicated concentrations (average  $\pm$  s.d., n=3). **(g)** Microtubule organization in fixed HeLa-WT cells treated for 4 hours with spastazoline (10  $\mu$ M) or DMSO (0.1%) and stained for  $\alpha$ -tubulin. Representative images, identically contrasted maximum intensity projections of four planes of the Z-stacks from two independent experiments are shown. Scale bar =10  $\mu$ m. **(h)** SDS-PAGE analysis of a purified recombinant human VPS4B construct (Coomassie blue, gel for purified protein was run at least twice). **(i)** Steady-state ATPase activity of the VPS4B construct in the presence of spastazoline at the indicated concentrations (1 mM MgATP, average  $\pm$  s.d., n = 3). **(j)** Confocal fluorescence-based analysis of GFP signal during cell division in doxycycline-induced live HeLa-N386C cells (0.2% DMSO was used as solvent control). Cells were imaged every 2 min. Graph shows the number of GFP-dots detected during 30 min from when ingression of the cleavage furrow was first observed (t=0 min). Cells (n=7) from three independent experiments were analyzed (average  $\pm$  s.d.).